This is the peer-reviewed, final accepted version for American Mineralogist, published by the Mineralogical Society of America.
The published version is subject to change. Cite as Authors (Year) Title. American Mineralogist, in press.
DOI: https://doi.org/10.2138/am-2023-9133. http://www.minsocam.org/

Calorimetry and structural analysis of uranyl sulfates with rare topologies

Samuel N. Perry[1], Arkin Kurama[1], Maximilian Martin[1] and Peter C. Burns[1,2*]

[1]Department of Civil and Environmental Engineering and Earth Sciences, University of Notre Dame, Notre Dame, IN, 46556, USA

[2]Department of Chemistry and Biochemistry, University of Notre Dame, Notre Dame, IN, 46556, USA

Abstract

Uranyl sulfate minerals are the most rapidly expanding group of uranium minerals, with dozens of species described in the past decade from the localities of White Canyon, USA and Jáchymov, Czech Republic. Synthetic analogs of a suite of uranyl sulfate minerals were crystallized, characterized, and the standard-state enthalpies of formation ($\Delta H_f°$) were determined. Synthetic lussierite is monoclinic, space group *Cc*, a = 9.2896, b = 28.685, c = 9.6155, β = 93.504. Synthetic geschieberite is orthorhombic, space group $Pna2_1$, a = 13.7408, b = 7.2713, c = 11.5844. The standard-state enthalpies of formation from the binary oxides for lussierite, péligotite, shumwayite, geschieberite, and bluelizardite are -3214 ± 78, -2026 ± 33, -587 ± 22, -966.1 ± 10.9, and -2084 ± 21 kJ/mol, respectively, while the standard-state enthalpies of formation of each phase from its elements are -9743 ± 78, -7220 ± 33, -5255 ± 22, -3916 ± 20, and -7117 ± 21 kJ/mol, respectively. The $\Delta H_f°$ of péligotite was accurately estimated using the $\Delta H_f°$ of lussierite, bluelizardite and literature values of the oxide components of each phase. This implies that estimates can be made accurately of the $\Delta H_f°$ of uranyl sulfates of minerals without

Corresponding author: Pburns@nd.edu

synthetic analogs.

Keywords:

High temperature drop solution calorimetry; uranyl sulfate minerals; hydrogen atom positions

Introduction

Uranium is of considerable societal importance: it is the primary fuel of nuclear energy, essential for production of many medical isotopes, central to international security concerns regarding nuclear weapons and non-proliferation, and an environmental contaminant where uranium mining and nuclear fuel cycle activities occurred. Uranyl sulfates, which contain U in its hexavalent oxidation state as the UO_2^{2+} uranyl ion, are an important and rapidly growing group of secondary minerals found where hydration-oxidation processes alter primary uranium minerals and sulfides, typically in abandoned mines (Finch and Murakami, 1999; Plášil et al., 2014). Acid-mine drainage conditions promote the transport of UO_2^{2+} and SO_4^{2+} aqueous ions through the country rock, resulting in efflorescent crusts of secondary minerals on mine walls (Kampf et al., 2019). Until 2009, less than 20 uranyl sulfate minerals had been described, of which zippeite ($K_3(H_2O)_{3.3}[(UO_2)_4(SO_4)_2O_3(OH)]$) is the most commonly encountered. Over the past dozen years studies of mining districts including White Canyon, Utah, USA, and Jáchymov, Czech Republic, have tripled the number of described uranyl sulfate mineral species (IMA, 2023).

The structures of uranyl sulfate minerals generally consist of anionic structural units containing uranyl and sulfate polyhedra and an interstitial complex of low-valence cations and H_2O (Burns et al., 1997). Uranyl oxyanion structural units in uranyl minerals have been organized into a hierarchy based on dimensionality (Burns et al., 1996; Krivovichev and Plášil, 2013), in which sheets predominate (Burns et al., 1996). The structural units of uranyl sulfate minerals are topologically and dimensionally diverse, including finite clusters, chains, and sheets of polyhedra (Gurzhiy and Plášil, 2019). Sulfate groups bond to uranyl ions in both monodentate

This is the peer-reviewed, final accepted version for American Mineralogist, published by the Mineralogical Society of America.
The published version is subject to change. Cite as Authors (Year) Title. American Mineralogist, in press.
DOI: https://doi.org/10.2138/am-2023-9133. http://www.minsocam.org/

and bidentate fashions, which further enhances structural diversity through the multiple modes of connection between the polyhedra (Krivovichev and Plášil, 2013; Gurzhiy and Plášil, 2019). No thermodynamic data exists to help understand the formation of the unique uranyl sulfates found in White Canyon, Utah.

High-temperature oxide melt solution calorimetry has been extensively applied for determination of the enthalpy of formation ($\Delta H_f°$) of uranyl compounds (Navrotsky, 2014) including uranyl silicates (boltwoodite, uranophane (Shvareva et al., 2011); soddyite (Gorman-Lewis et al., 2007)), uranyl carbonates (rutherfordine, grimselite, andersonite (Kubatko et al., 2005)), uranyl vanadates (carnotite, curienite, francevillite (Spano et al., 2017)), uranyl sulfates (zippeite (Sharifironizi et al., 2016); natrozippeite, cobaltzippeite, zinczippeite (Sharifironizi and Burns, 2018)), and some U^{IV} minerals (coffinite (Guo et al., 2015); brannerite (Simoncic and Navrotsky, 2007); behounekite (Zhang et al., 2019)). These studies revealed relationships between the enthalpy of formation and the Smith acidity of the interstitial cation (Sharifironizi and Burns, 2018), the normalized charge deficiency per anion (Spano et al., 2017), and the number of oxygen atoms per U (Navrotsky et al., 2013).

Table 1. The concentration and quantity of each reagent used in the phase synthesis.

Name	Formula	H_2O (ml)	UO_3 (g)	18.4 M H_2SO_4 (mL)	Aliquot evaporated (mL)	5.0 M NaOH (mL)	Final Stock pH
Lussierite	$Na_{10}[(UO_2)(SO_4)_4](SO_4)_2 \cdot 3H_2O$	20.0	2.6	2.2	3	‡	2.6
Péligotite	$Na_6[(UO_2)(SO_4)_4] \cdot 4H_2O$	40.0	5.7	4.5	2	1.15*	2.5
Shumwayite	$[(UO_2)(SO_4)(H_2O)_2]_2 \cdot H_2O$	20.0	1.4	0.3	2	None	1.7
Bluelizardite	$Na_7[(UO_2)(SO_4)_4]Cl \cdot 2H_2O$	20.0	5.1	8.6	3	26.4†	1.8

Name	Formula	H_2O (ml)	$(UO_2)(NO_3)_2 \cdot 6H_2O$ (g)	18.4 M H_2SO_4 (mL)	K_2SO_4 (g)
Geschieberite	$K_2[(UO_2)(SO_4)_2(H_2O)] \cdot H_2O$	5.0	2.5	0.14	0.44

*NaOH added to aliquot vial rather than the stock solution.
†5 M solution was added to the uranyl sulfate stock, followed by 2.5 mL of 12 M HCl to adjust the pH.
‡The solution was titrated with NaOH to a specific pH and the volume was not recorded.

Here we report synthesis of the analogs of five of the new uranyl sulfate minerals from Red Canyon and Jáchymov and determination of their enthalpies of formation. We had initially planned to measure the aqueous solubility of these minerals, but we qualitatively observed that these phases are highly soluble and accurate measurements were precluded by the large amount of material those measurements would require. This is part of our on-going efforts to develop thermodynamic data for uranyl minerals in order to better understand their occurrences and transformations.

Methods

Synthesis of uranyl sulfate phases. Lab-prepared UO_3 was synthesized by placing $(UO_2)(NO_3)_2 \cdot 6H_2O$ (International Bio-analytical Industries) into an alumina crucible, covering the crucible with a watch glass and heating the sample to 600 ˚C on a hot plate in a hood until the uranyl nitrate had melted and then formed a red-orange solid. The material was verified as slightly hydrated UO_3 via powder X–ray diffraction (PDF-00-053-0877) and was stored in a sealed container under vacuum until used as a reagent.

Crystalline uranyl sulfate phases were synthesized from aqueous uranyl sulfate stock solutions containing various amounts of ultrapure Milli–Q H_2O, UO_3 and concentrated H_2SO_4 (BDH). Different amounts of 5 M NaOH (ACS) were added to supply sodium ions and to adjust the pH. Details of the synthesis experiments are summarized in Table 1. The pH of each solution was measured using a Fisher Scientific AB150 pH/mV probe calibrated with three NIST standards (BDH). To synthesize the analog of bluelizardite, $Na_7[(UO_2)(SO_4)_4]Cl \cdot 2H_2O$, 5 M NaOH was added to a uranyl sulfate solution until a precipitate formed. The precipitate was then

This is the peer-reviewed, final accepted version for American Mineralogist, published by the Mineralogical Society of America.
The published version is subject to change. Cite as Authors (Year) Title. American Mineralogist, in press.
DOI: https://doi.org/10.2138/am-2023-9133. http://www.minsocam.org/

dissolved by adding concentrated HCl (BDH). The solutions that yielded synthetic analogs of lussierite, shumwayite and bluelizardite were evaporated in Isotemp ovens at 60, 70 and 70 ˚C, respectively, until crystals formed at the bottom of the vials and a small amount of the stock solution remained. The solution that yielded the synthetic analog of péligotite was dried to completion at 70 ˚C. After addition of K_2SO_4 (Fisher Chemical), geschieberite crystals precipitated from the stock solution at room temperature over a few hours and were harvested quickly from the mother liquor to prevent contamination by the formation of secondary potassium sulfate salts. Crystals from all syntheses were harvested and rinsed with ethanol and a few drops of hot ultrapure water on filter paper in a Buchner funnel to remove any impurities or residual stock solution, if present. A vacuum was applied during rinsing to prevent excessive dissolution of the uranyl sulfate crystals. After cleaning, all crystals were dried completely over the vacuum, then recovered for further analysis.

Table 2. Crystallographic parameters of synthetic phases examined in this study.

	Lussierite	**Péligotite**	**Shumwayite**	**Geschieberite**	**Bluelizardite**
Space Group	*C*c	*P*-1	$P2_1/c$	$Pna2_1$	$C2/c$
***a* (Å)**	9.2896	9.7935	6.730	13.7408	21.162
***b* (Å)**	28.685	9.9419	12.479	7.2713	5.3462
***c* (Å)**	9.6155	10.615	16.881	11.5844	34.719
α (°)	90	88.659	90	90	90
β (°)	93.504	74.013	90.931	90	104.902
γ (°)	90	89.188	90	90	90
Vol (Å^3)	2557.4	993.26	1417.5	1157.43	3795.9

Single Crystal X–ray Diffraction. Selected crystals from each product were immersed in mineral oil and attached to cryoloops. Single-crystal X–ray diffraction (SC–XRD) data were collected using a Bruker Apex II Quazar diffractometer with a micro-source sealed tube using monochromated Mo *Kα* X–radiation. Data integration was done with the APEX III software and

SADABS was used to apply absorption corrections (Sheldrick, 2008). All structures were solved and refined with the SHELXTL software package (Sheldrick, 2015a, b). The synthetic phases in this study diffracted well enough that the positions of all hydrogen atoms were determined. Hydrogen atoms were added to all structures at crystallographically appropriate positions based on residual electron densities. Crystallographic information files (CIF) were generated and were used to simulate powder diffractograms (Macrae et al., 2020). Crystallographic information is summarized in Table 2.

Powder X–ray Diffraction. Dried crystals of each phase were ground into a fine powder using an agate mortar and pestle. Small amounts of powder were placed on a glass slide for collection of diffraction data using a Bruker D8 Advance Davinci powder X–ray diffractometer (PXRD). Data were collected using monochromatic Cu Kα radiation over the 2θ range of 5 to 55°. Powder patterns of each uranyl sulfate phase were simulated using the Mercury software package (Macrae et al., 2020) using the structural parameters of the synthetic phases obtained during the SC–XRD analysis. Comparison of simulated and measured diffractograms of the bulk powders confirmed phase identity and purity.

Inductively Coupled Plasma Optical Emission Spectroscopy. For verification of the cation content of the phases under study, 10 mg of each powdered phase were dissolved in 5% v/v nitric acid that was analyzed in an Avio 200 PerkinElmer inductively coupled plasma optical emission spectrometer (ICP–OES). Each phase was analyzed in triplicate with five calibration standards, with Y used as an internal standard. The resulting compositions are in good agreement

with the ideal chemical formulas from the literature and increase our confidence that the synthetic phases are identical to the natural minerals.

Thermogravimetric Analysis. Thermogravimetric analysis (TGA) was performed using ~12 mg of each powdered phase in alumina crucibles, with an empty crucible as a blank, inside a Mettler Toledo Thermogravimetric Analyzer heated to 700 ºC. Bluelizardite was heated to 800 ºC, although the Cl was completely liberated by ~725 ºC. The moles of water of each phase, and Cl in the case of bluelizardite, were calculated from the mass loss of the sample as measured by the TGA.

Calorimetry. A Setaram AlexSYS 1000 model Calvet high temperature calorimeter was used to measure the heat of dissolution of each crystalline phase. Each powdered phase was pressed into ~5 mg pellets and dropped into molten solvent at 700 ºC. Sodium molybdate ($3Na_2O{\cdot}4MoO_3$) was employed as the solvent as it is an effective solvent for uranyl phases, including uranyl sulfates (Navrotsky, 1997, 2014; Sharifironizi et al., 2016; Sharifironizi and Burns, 2018). Prior to calorimetric studies, pellets of each phase were dropped into molten sodium molybdate in alumina pans in a furnace at 700 ºC to visually confirm complete dissolution of the pellet. In the calorimeter, oxygen gas was bubbled through the solvent to maintain oxidizing conditions and to stir the solvent to encourage dissolution of the pellets. Oxygen flushing gas was used to sweep away gas and water vapor from the crucible. The heat of dissolution of each phase was recorded and used in thermal chemical cycles to calculate the enthalpies of formation of each compound from elements and binary oxides. The thermal chemical cycles and number of drops for each phase are listed in Table 3.

153 For bluelizardite, the distribution of Cl between the solvent and gas upon dissolution at
154 700 ºC was determined (Lilova et al., 2020). The ΔH_{ds} of NaCl was measured by dropping 5 mg
155 pellets of ground reagent-grade NaCl (Fisher Chemical) into solvent in the calorimeter and
156 recording the heat of dissolution. Powdered NaCl was heated in a TGA and no mass loss was
157 observed at or below 700 °C, indicating the reagent had not absorbed ambient water. To verify
158 that Cl remained in the solvent during dissolution, alumina crucibles were prepared with 1 g of
159 freshly prepared sodium molybdate solvent in a furnace at 700 ºC. Fifty mg of NaCl was added
160 (30.3 mg Cl) to four crucibles. After quenching the total mass loss was 3.7 ± 1.7 mg, which was
161 comparable to the mass lost in a blank crucible loaded with only sodium molybdate solvent.
162 Analysis of the quenched solvent with SEM-EDS indicated the presence of Cl (Table S5).
163
164
165 **Results and Discussion**

166 The refined crystal structures of the five uranyl sulfate phases under study are in good
167 accord with the published structures of the natural phases (Table 2) (Plášil et al., 2014; Plášil et
168 al., 2015; Kampf et al., 2017a; Kampf et al., 2017b; Kampf et al., 2019). Powder X–ray
169 diffraction data confirmed the identity and purity of each phase (Fig. S1-S5). Chemical analysis
170 yielded molar ratios of M:U:S (M = Na, K or no cation) within error of the ideal mineral
171 formulas (Table S1). Thermogravimetric analysis provided the molar amounts of water and Cl of
172 the synthetic uranyl sulfates and these are in agreement with the idealized mineral formulas

173 (Table S2).

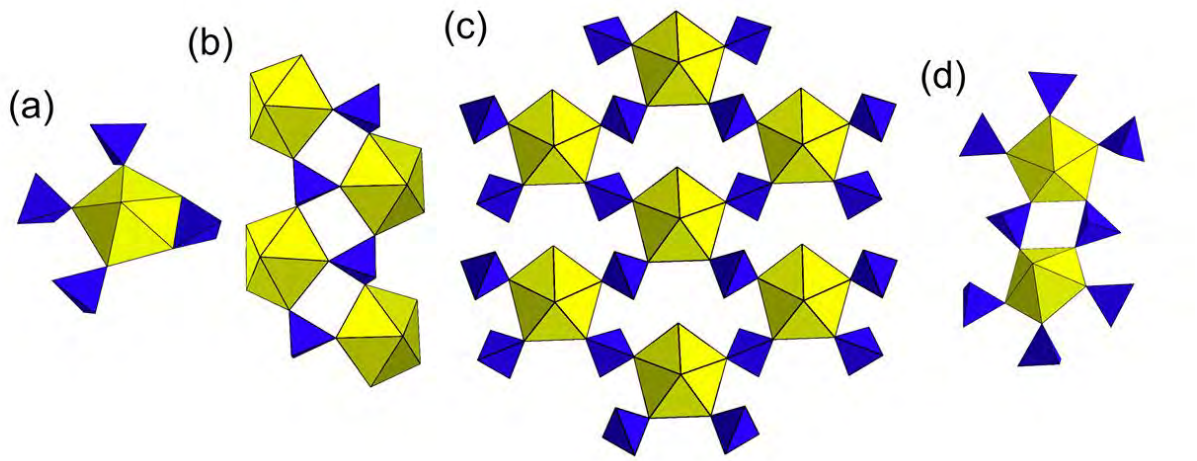

Fig. 1. The uranyl sulfate structural units for (a) péligotite and lussierite, (b) shumwayite, (c) geschieberite and (d) bluelizardite.

174

175 The structural units of the five compounds under study are shown in Fig. 1. The earlier
176 crystal structure determinations for natural samples of geschieberite and lussierite did not include
177 the positions of H atoms. The X–ray data for the synthetic crystals readily yielded the positions
178 of all H atoms. In the case of geschieberite, Plášil et al. proposed H bonds donated by the H_2O
179 group bonded in the equatorial plane of the uranyl ion and accepted by non-bridging O atoms of
180 sulfate tetrahedra located in the same sheet as the uranyl polyhedron. There are two H_2O groups
181 in the structure: the one bonded to the uranyl ion, and another located in the interlayer where it is
182 bonded to K. In the new structure, the H bonds of the H_2O group bonded to the uranyl do form
183 the predicted bonds to the sulfate groups (Fig. 2, O7). However, in the synthetic structure the
184 H_2O group bonded to the uranyl ion also accepts a H bond donated by the H_2O group located in
185 the interlayer (Fig. 2, O12). The other H bond emanating from the interlayer H_2O group is
186 accepted by a uranyl ion oxygen atom of an adjacent sheet, such that H bonds from this
187 interlayer H_2O group bridge sheets of uranyl and sulfate polyhedra (Fig. 2).

188

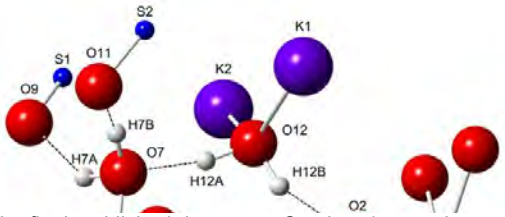

This is the peer-reviewed, final accepted version for American Mineralogist, published by the Mineralogical Society of America.
The published version is subject to change. Cite as Authors (Year) Title. American Mineralogist, in press.
DOI: https://doi.org/10.2138/am-2023-9133. http://www.minsocam.org/

The structure of lussierite contains three H_2O groups located in interstitial positions, where each of them is bonded to two Na cations (Fig. 3). The structural unit consists of a uranyl polyhedron sharing vertices with four sulfate tetrahedra, and there are two different sulfate tetrahedra in the interstitial complex. The O27 oxygen donates two H bonds that are accepted by two different interstitial oxygen atoms of sulfate groups. The O28 oxygen atom donates H bonds that are accepted by oxygen atoms of two sulfate tetrahedra of different structural units. As for the O27 oxygen, O29 oxygen donates two H bonds that are accepted by oxygen atoms of the two distinct interstitial sulfate groups (Fig. 3).

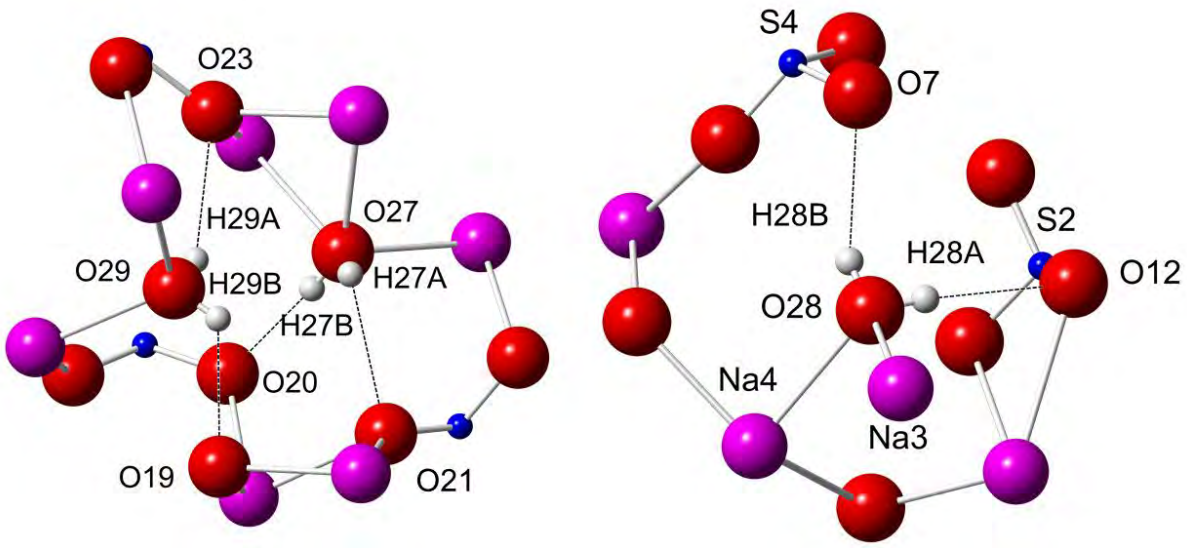

Fig. 3. The hydrogen bonding in lussierite. (Left) The O27 water molecule donates hydrogen bonds to two different interstitial oxygen atoms of sulfate units. (Left) The O29 water molecule also donates hydrogen bonds to oxygen atoms of two distinct, interstitial sulfate units. (Right) The O28 water molecule donates hydrogen bonds that connect to two distinct sulfate tetrahedra

212

213

214

215

216

217 Thermodynamic cycles (Table 3) were used to calculate the standard-state enthalpy of
218 formation of each phase from the measured heats of dissolution. When sufficient sample was
219 available, additional measurements were done using a second AlexSYS calorimeter to verify
220 heat curve data. The standard-state enthalpies of formation from the binary oxides for lussierite,
221 péligotite, shumwayite, geschieberite, and bluelizardite are -3214 ± 78, -2026 ± 33, -587 ± 22, -
222 966.1 ± 10.9, and -2084 ± 21 kJ/mol, respectively. The standard-state enthalpies of formation of
223 each phase from its elements are -9743 ± 78, -7220 ± 33, -5255 ± 22, -3916 ± 20, and -7117 ± 21
224 kJ/mol, respectively.

225 Péligotite, lussierite and bluelizardite are structurally and chemically similar minerals,
226 which provides an opportunity to evaluate the internal consistency of the calorimetric results.
227 Each contains finite uranyl sulfate units linked through interstitial Na and H_2O, although
228 bluelizardite has Cl in the interstitial complex, and lussierite contains sulfate groups in the
229 interstitial complex. Literature values for $\Delta H_f°$ for H_2O, NaCl, and Na_2SO_4 are -285.5, -411.3,
230 and -1387.8 kJ/mol, respectively (Robie et al., 1978). The $\Delta H_f°$ for péligotite,
231 $Na_6[(UO_2)(SO_4)_4](H_2O)_4$, calculated from the thermochemical cycles is -7220 ± 33 kJ/mol. This
232 value can also be estimated starting with $\Delta H_f°$ (-9743 ± 78 kJ/mol) of lussierite,
233 $Na_{10}[(UO_2)(SO_4)_4](SO_4)_2 \cdot 3H_2O$, by subtracting $\Delta H_f°$ for two moles of Na_2SO_4 and adding $\Delta H_f°$
234 for one mole of H_2O, which yields -7253 ± 78 kJ/mol. Similarly, it can be estimated starting with

This is the peer-reviewed, final accepted version for American Mineralogist, published by the Mineralogical Society of America.
The published version is subject to change. Cite as Authors (Year) Title. American Mineralogist, in press.
DOI: https://doi.org/10.2138/am-2023-9133. http://www.minsocam.org/

$\Delta H_f°$ (-7117 ± 21 kJ/mol) of bluelizardite, $Na_7[(UO_2)(SO_4)_4]Cl·2H_2O$, followed by subtracting the $\Delta H_f°$ of one mole of NaCl and adding the $\Delta H_f°$ of two moles of H_2O, which yields -7277 ± 21 kJ/mol.

Implications

Generally, SCXRD data for new minerals is collected on the X-ray diffractometer at room temperature, ~20 °C. Excepting for phases unstable at room temperature, it is normally no issue to determine the true structure of a mineral with modern diffractometers due to incremental improvements in detector resolution and X-ray sources. However, heavy elements such as U cause excessive X-ray scattering that can make accurately determining the thermal parameters of light elements as heavy as even O quite difficult. Exact H atom positions are often impossible to determine from natural uranium minerals and often the H-bond network must be estimated from bond valence calculations. This is further complicated by hydrous minerals that have dehydrated in the field prior to collection. Synthesis of uranyl mineral analogs in laboratory conditions avoids the dehydration issue with natural samples. Further, using a cryostream will both stabilize phases prone to dehydration and will reduce the X-ray scatter around U atoms such that H-atom positions can be more readily found, as exemplified by the phases reported in this study.

The $\Delta H_f°$ value of péligotite calculated from thermochemical cycles in this study is in close agreement with the $\Delta H_f°$ calculated from the starting $\Delta H_f°$ of similar minerals. This implies that estimating the $\Delta H_f°$ values can be done for minerals that have yet to be synthesized in laboratory conditions. For instance, ottohahnite, $Na_6(UO_2)_2(SO_4)_5(H_2O)_7·1.5H_2O$, is structurally similar to péligotite, lussierite and bluelizardite. Ottohahnite has no synthetic analog and its enthalpy of formation is unknown, but using the $\Delta H_f°$ of péligotite and literature enthalpy values

an estimate can be made of the $\Delta H_f°$ of ottohahnite. The literature value of $\Delta H_f°$ for $UO_2SO_4 \cdot 3H_2O$ is -2747.2 kJ/mol (Glushko, 1978; Karyakin et al., 2003). Starting with $\Delta H_f°$ of -7220 ± 33 kJ/mol, then adding $\Delta H_f°$ for one mole of $UO_2SO_4 \cdot 3H_2O$ and $\Delta H_f°$ for 1.5 moles of H_2O yields -10,395.5± 33 kJ/mol for ottohahnite.

The rate of new mineral discoveries, particularly uranyl sulfates, is far outpacing the rate at which analogs of minerals are being synthesized in laboratories. The newly described uranyl sulfate minerals are diverse in structure and chemistry, indicating variations in local geochemical conditions. However, aside from the minerals described in this study and a few others, most of the uranyl sulfates have not been replicated in laboratory conditions and their thermodynamic data is unknown. The lack of $\Delta H_f°$ data of these new minerals hampers a deeper understanding of the formation processes behind these minerals. Previous efforts have been made to accurately estimate the $\Delta H_f°$ values of uranyl minerals without experiment analysis or expensive DFT simulations (Chen et al., 1999). The results of this study imply that accurate estimates can be made of the $\Delta H_f°$ values of mineral phases by using $\Delta H_f°$ values from chemically and structurally similar phases. This is not only accurate, but rapid and facile. This method will likely be improved with more data points for study.

The standard state entropy of formation for zippeite is three orders of magnitude smaller than the standard state enthalpy of formation (Sharifironizi and Burns, 2018; Sharifironizi et al., 2016), indicating that the standard state enthalpy is the largest contributor to the standard state free energy of the mineral. If that is the case for other uranyl sulfates, then estimating $\Delta H_f°$ of a mineral using the method described here also allows for an accurate approximation of the $\Delta G_f°$. This is of potential value, as the high solubility of this suite of uranyl sulfates prevented experimental determination of their solubility products. Geochemists that model uranium mineral

formation and uranium transport in acid mine conditions may therefore be interested in a means of predicting the $\Delta G_f°$ of uranyl sulfate minerals that exist in defunct uranium mines, but have yet to be replicated in a laboratory.

Notes:

The authors declare no competing interests.

Acknowledgements

This work was supported by funding from the University of Notre.

288

This is the peer-reviewed, final accepted version for American Mineralogist, published by the Mineralogical Society of America.
The published version is subject to change. Cite as Authors (Year) Title. American Mineralogist, in press.
DOI: https://doi.org/10.2138/am-2023-9133. http://www.minsocam.org/

Table 3. Calorimetry thermal cycles for determination of enthalpy of formation ($\Delta H_f°$). The number of calorimeter drops is indicated in parenthesis in the kJ·mol^{-1} column. Crystalline phase = xl; gas phase = g; solution = soln; liquid phase = l. The error was calculated as two standard deviations of the mean.

Reactions	Compound	Thermal Equation	kJ·mol^{-1}	Reference
ΔH1	ΔH_{ds} Lussierite	$Na_{10}[(UO_2)(SO_4)_4](SO_4)_2{\cdot}3(H_2O)_{(xl,\ 298\ K)} = 5Na_2O_{(soln,\ 973\ K)} + UO_{3\ (soln,\ 973\ K)} + 6SO_{3\ (soln,\ 973\ K)} + 3H_2O_{(g,\ 973\ K)}$	1120 ± 71 (5)	This study
ΔH2	ΔH_{ds} Péligotite	$Na_6[(UO_2)(SO_4)_4]{\cdot}4H_2O_{(xl,\ 298\ K)} = 3Na_2O_{(soln,\ 973\ K)} + UO_{3\ (soln,\ 973\ K)} + 4SO_{3\ (soln,\ 973\ K)} + 4H_2O_{(g,\ 973\ K)}$	844 ± 25 (6)	This study
ΔH3	ΔH_{ds} Shumwayite	$[(UO_2)(SO_4)(H_2O)_2]_2{\cdot}H_2O_{(xl,\ 298\ K)} = 2UO_{3\ (soln,\ 976\ K)} + 2SO_{3\ (soln,\ 976\ K)} + 5H_2O_{(soln,\ 976\ K)}$	542 ± 14 (18)	This study
ΔH4	ΔH_{ds} Geschieberite	$K_2[(UO_2)(SO_4)_2]{\cdot}2(H_2O)_{(xl,\ 298\ K)} = 1K_2O_{(soln,\ 973\ K)} + 1UO_{3\ (soln,\ 973\ K)} + 2SO_{3\ (soln,\ 973\ K)} + 2H_2O_{(g,\ 973\ K)}$	388 ± 6 (16)	This study
ΔH5	ΔH_{ds} Bluelizardite	$Na_7[(UO_2)(SO_4)_4]Cl{\cdot}2(H_2O)_{(xl,\ 298\ K)} = 3Na_2O_{(soln,\ 973\ K)} + UO_{3\ (soln,\ 973\ K)} + 4SO_{3\ (soln,\ 973\ K)} + NaCl_{(soln,\ 973\ K)} + 2H_2O_{(g,\ 973\ K)}$	838.2 ± 1.9 (9)	This study
ΔH7	ΔH_{ds} (UO_3)	$UO_{3\ (xl,\ 298\ K)} = UO_{3\ (soln,\ 973\ K)}$	9.5 ± 1.5	Helean et al. 2002
ΔH8	ΔH_{ds} (SO_3)	$SO_{3\ (g,\ 298\ K)} = SO_{3\ (soln,\ 973\ K)}$	-203.7 ± 4.1	Navrotsky 2014
ΔH9	ΔH_{ds} (Na_2O)	$Na_2O_{(xl,\ 298\ K)} = Na_2O_{(soln,\ 973\ K)}$	-217.6 ± 4.3	Tessier et al. 2000
ΔH10	ΔH_{ds} (K_2O)	$K_2O_{(xl,\ 298\ K)} = K_2O_{(soln,\ 973\ K)}$	-318 ± 3	Tessier et al. 2000
ΔH11	ΔH_{ds} (NaCl)	$NaCl_{(xl,\ 298\ K)} = NaCl_{(soln,\ 973\ K)}$	74.6 ± 1.1 (6)	This study
ΔH12	ΔH_{hc} (H_2O)	$H_2O_{(l,\ 298\ K)} = H_2O_{(g,\ 973\ K)}$	69.01	Robie et al. 1978
ΔH13	$\Delta H_f°$ (UO_3)	$U_{(xl,\ 298\ K)} + 1.5O_{2\ (g,\ 298\ K)} = UO_{3\ (xl,\ 298\ K)}$	-1223.8 ± 0.8	Robie et al. 1978
ΔH14	$\Delta H_f°$ (SO_3)	$S_{(xl,\ 298\ K)} + 1.5O_{2\ (g,\ 298\ K)} = SO_{3\ (g,\ 298\ K)}$	-395.7 ± 0.7	Robie et al. 1978
ΔH15	$\Delta H_f°$ (Na_2O)	$2Na_{(xl,\ 298\ K)} + 0.5O_{2\ (g,\ 298\ K)} = Na_2O_{(xl,\ 298\ K)}$	-414.8 ± 0.3	Robie et al. 1978
ΔH16	$\Delta H_f°$ (K_2O)	$2K_{(xl,\ 298\ K)} + 0.5O_{2\ (g,\ 298\ K)} = K_2O_{(xl,\ 298\ K)}$	-363.2 ± 2.1	Robie et al. 1978
ΔH17	$\Delta H_f°$ (NaCl)	$Na_{(xl,\ 298\ K)} + 0.5Cl_{2\ (g,\ 298\ K)} = NaCl_{(xl,\ 298\ K)}$	-411.30 ± 0.10	Robie et al. 1978
ΔH18	$\Delta H_f°$ (H_2O)	$H_{2\ (g,\ 298\ K)} + 0.5O_{2\ (g,\ 298\ K)} = H_2O_{(l,\ 298\ K)}$	-285.80 ± 0.10	Robie et al. 1978
ΔH19	$\Delta H_{f\text{-}ox}°$ Lussierite	$5Na_2O_{(xl,\ 298\ K)} + UO_{3\ (xl,\ 298\ K)} + 6SO_{3\ (xl,\ 298\ K)} + 3H_2O_{(l,\ 298\ K)}$ $-\Delta H1 + 5\Delta H9 + 1\Delta H7 + 6\Delta H8 + 3\Delta H12$	-3214 ± 78	
ΔH20	$\Delta H_f°$ Lussierite	$10Na_{(xl,\ 298\ K)} + U_{(xl,\ 298\ K)} + 6S_{(xl,\ 298\ K)} + 3H_{2\ (g,\ 298\ K)} + 14.5O_{2\ (g,\ 298\ K)}$ $-\Delta H1 + 5\Delta H9 + 1\Delta H7 + 6\Delta H8 + 3\Delta H12 + 5\Delta H15 + 1\Delta H13 + 6\Delta H14 + 3\Delta H18$	-9743 ± 78	
ΔH21	$\Delta H_{f\text{-}ox}°$ Péligotite	$3Na_2O_{(xl,\ 298\ K)} + UO_{3\ (xl,\ 298\ K)} + 4SO_{3\ (xl,\ 298\ K)} + 4H_2O_{(l,\ 298\ K)}$ $-\Delta H2 + 3\Delta H9 + 1\Delta H7 + 4\Delta H8 + 4\Delta H12$	-2026 ± 33	
ΔH22	$\Delta H_f°$ Péligotite	$6Na_{(xl,\ 298\ K)} + U_{(xl,\ 298\ K)} + 4S_{(xl,\ 298\ K)} + 4H_{2\ (g,\ 298\ K)} + 11O_{2\ (g,\ 298\ K)}$ $-\Delta H2 + 3\Delta H9 + 1\Delta H7 + 4\Delta H8 + 4\Delta H12 + 3\Delta H15 + 1\Delta H13 + 4\Delta H14 + 4\Delta H18$	-7220 ± 33	
ΔH23	$\Delta H_{f\text{-}ox}°$ Shumwayite	$2UO_{3\ (xl,\ 298\ K)} + 2SO_{3\ (xl,\ 298\ K)} + 5H_2O_{(l,\ 298\ K)}$ $-\Delta H3 + 2\Delta H7 + 2\Delta H8 + 5\Delta H12$	-587 ± 22	
ΔH24	$\Delta H_f°$ Shumwayite	$2U_{(xl,\ 298\ K)} + 2S_{(xl,\ 298\ K)} + 5H_{2\ (g,\ 298\ K)} + 8.5O_{2\ (g,\ 298\ K)}$ $-\Delta H3 + 2\Delta H7 + 2\Delta H8 + 5\Delta H12 + 2\Delta H13 + 2\Delta H14 + 5\Delta H18$	-5255 ± 22	

This is the peer-reviewed, final accepted version for American Mineralogist, published by the Mineralogical Society of America.
The published version is subject to change. Cite as Authors (Year) Title. American Mineralogist, in press.
DOI: https://doi.org/10.2138/am-2023-9133. http://www.minsocam.org/

ΔH25	$\Delta H_{f\text{-}ox}°$ Geschieberite	$1K_2O_{(xl,\ 298\ K)} + UO_{3\ (xl,\ 298\ K)} + 2SO_{3\ (xl,\ 298\ K)} + 2H_2O_{(l,\ 298\ K)}$ $-\Delta H4 + 1\Delta H10 + 1\Delta H7 + 2\Delta H8 + 2\Delta H12$	-966 ± 11
ΔH26	$\Delta H_f°$ Geschieberite	$2K_{(xl,\ 298\ K)} + U_{(xl,\ 298\ K)} + 2S_{(xl,\ 298\ K)} + 2H_{2\ (g,\ 298\ K)} + 12O_{2\ (g,\ 298\ K)}$ $-\Delta H4 + 1\Delta H10 + 1\Delta H7 + 2\Delta H8 + 2\Delta H12 + 1\Delta H16 + 1\Delta H13 + 2\Delta H14 + 2\Delta H18$	-3916 ± 20
ΔH27	$\Delta H_{f\text{-}ox}{}^0$ Bluelizardite	$3Na_2O_{(xl,\ 298\ K)} + UO_{3\ (xl,\ 298\ K)} + 4SO_{3\ (xl,\ 298\ K)} + NaCl_{(xl,\ 298\ K)} + 2H_2O_{(l,\ 298\ K)}$ $-\Delta H5 + 3\Delta H9 + 1\Delta H7 + 4\Delta H8 + 1\Delta H11 + 2\Delta H12$	-2084 ± 21
ΔH28	$\Delta H_f°$ Bluelizardite	$7Na_{(xl,\ 298\ K)} + U_{(xl,\ 298\ K)} + 4S_{(xl,\ 298\ K)} + 0.5Cl_{2\ (g,\ 298\ K)} + 2H_{2\ (g,\ 298\ K)} + 10O_{2\ (g,\ 298\ K)}$ $-\Delta H5 + 3\Delta H9 + 1\Delta H7 + 4\Delta H8 + 1\Delta H11 + 2\Delta H12 + 3\Delta H15 + 1\Delta H13 + 4\Delta H14 + 1\Delta H17 + 2\Delta H18$	-7117 ± 21

References

Burns, P.C., Ewing, R.C. and Hawthorne, F.C. (1997) The crystal chemistry of hexavalent uranium: Polyhedron geometries, bond-valence parameters, and polymerization of polyhedra. *The Canadian Mineralogist*, **35**, 1551-1570.

Burns, P.C., Miller, M.L. and Ewing, R.C. (1996) U^{6+} minerals and inorganic phases: A comparison and hierarchy of crystal structures. *The Canadian Mineralogist*, **34**, 845-880.

Finch, R. and Murakami, T. (1999) Systematics and paragenesis of uranium minerals. Pp. 91-179. in: *Uranium: Mineralogy, Geochemistry and the Environment* (P.C. Burns and R.C. Finch, editors). Reviews in Mineralogy, **38**. Mineralogical Society of America, Washington, DC.

(1978) *Termicheskie konstanty veshchestv* (Thermal Constants of Substances), Glushko, V.P., Ed., Moscow: Akad. Nauk SSSR, issue 8, part 1.

Gorman-Lewis, D., Mazeina, L., Fein, J.B., Szymanowski, J.E., Burns, P.C. and Navrotsky, A. (2007) Thermodynamic properties of soddyite from solubility and calorimetry measurements. *The Journal of Chemical Thermodynamics*, **39**, 568-575.

Guo, X., Szenknect, S., Mesbah, A., Labs, S., Clavier, N., Poinssot, C., Ushakov, S.V., Curtius, H., Bosbach, D., Ewing, R.C., Burns, P.C., Dacheux, N. and Navrotsky, A. (2015) Thermodynamics of formation of coffinite, $USiO_4$. *Proceedings of the National Academy of Sciences*, **112**, 6551-6555.

Gurzhiy, V.V. and Plášil, J. (2019) Structural complexity of natural uranyl sulfates. *Acta Crystallographica*, **B75**, 39-48.

Helean, K.B., Navrotsky, A., Vance, E.R., Carter, M.L., Ebbinghaus, B., Krikorian, O., Lian, J., Wang, L.M. and Catalano, J.G. (2002) Enthalpies of formation of Ce-pyrochlore, $Ca_{0.93}Ce_{1.00}Ti_{2.035}O_{7.00}$, U-pyrochlore, $Ca_{1.46}U^{4+}_{0.23}U^{6+}_{0.46}Ti_{1.85}O_{7.00}$ and Gd-pyrochlore, $Gd_2Ti_2O_7$: Three materials relevant to the proposed waste form for excess weapons plutonium. *Journal of Nuclear Materials*, **303**, 226-239.

International Mineralogical Association. (2023, Accessed June 1). International Mineralogical Association Database of Mineral Properties. https://rruff.info/ima/

Kampf, A.R., Olds, T.A., Plášil, J., Nash, B.P. and Marty, J. (2019) Lussierite, a new sodium uranyl sulfate mineral with bidentate UO_7–SO_4 linkage from the Blue Lizard mine, San Juan County, Utah, USA. *Mineralogical Magazine*, **83**, 799-808.

Kampf, A.R., Plášil, J., Kasatkin, A.V., Marty, J. and Čejka, J. (2017a) Klaprothite, péligotite and ottohahnite, three new minerals with bidentate UO_7–SO_4 linkages from the Blue Lizard mine, San Juan County, Utah, USA. *Mineralogical Magazine*, **81**, 753-779.

Kampf, A.R., Plášil, J., Kasatkin, A.V., Marty, J., Čejka, J. and Lapčák, L. (2017b) Shumwayite, $[(UO_2)(SO_4)(H_2O)_2]_2{\cdot}H_2O$, a new uranyl sulfate mineral from Red Canyon, San Juan County, Utah, USA. *Mineralogical Magazine*, **81**, 273-285.

329 Karyakin, N., Knyazev, A. and Gavrilova, S. (2003) Chemical thermodynamics of nickel,
330 copper, and zinc uranyl sulfates. *Radiochemistry*, **45**, 484-487.
331 Krivovichev, S.V. and Plášil, J. (2013) Mineralogy and crystallography of uranium. Pp. 15-119.
332 In: *Uranium, from Cradle to Grave* (P.C. Burns and G.E. Sigmon, editors). Mineralogical
333 Association of Canada Short Course, 43. Mineralogical Association of Canada, Québec,
334 Canada.
335 Kubatko, K.A., Helean, K.B., Navrotsky, A. and Burns, P.C. (2005) Thermodynamics of uranyl
336 minerals: Enthalpies of formation of rutherfordine, UO_2CO_3, andersonite,
337 $Na_2CaUO_2(CO_3)_3(H_2O)_5$, and grimselite, $K_3NaUO_2(CO_3)_3H_2O$. *American Mineralogist*,
338 **90**, 1284-1290.
339 Lilova, K., Pierce, E.M., Wu, L., Jubb, A.M., Subramani, T. and Navrotsky, A. (2020)
340 Energetics of salt-bearing sodalites, $Na_8Al_6Si_6O_{24}X_2$ (x= SO_4, ReO_4, Cl, I): A treatment
341 option for pertechnetate-enriched nuclear waste streams. *ACS Earth and Space*
342 *Chemistry*, **4**, 2153-2161.
343 Macrae, C.F., Sovago, I., Cottrell, S.J., Galek, P.T., McCabe, P., Pidcock, E., Platings, M.,
344 Shields, G.P., Stevens, J.S., Towler, M. and Wood, P.A. (2020) Mercury 4.0: From
345 visualization to analysis, design and prediction. *Journal of Applied Crystallography*, **53**,
346 226-235.
347 Navrotsky, A. (1997) Progress and new directions in high temperature calorimetry revisited.
348 *Physics and Chemistry of Minerals*, **24**, 222-241.
349 Navrotsky, A. (2014) Progress and new directions in calorimetry: A 2014 perspective. *Journal of*
350 *the American Ceramic Society*, **97**, 3349-3359.

Navrotsky, A., Shvareva, T., Guo, X. and Burns, P. (2013) Thermodynamics of uranium minerals and related materials. Pp. 147-164. In: *Uranium, from Cradle to Grave* (P.C. Burns and G.E. Sigmon, editors). Mineralogical Association of Canada Short Course, 43. Mineralogical Association of Canada, Québec, Canada.

Plášil, J., Hloušek, J., Kasatkin, A.V., Škoda, R., Novák, M. and Čejka, J. (2015) Geschieberite, $K_2(UO_2)(SO_4)_2(H_2O)_2$, a new uranyl sulfate mineral from Jáchymov. *Mineralogical Magazine*, **79**, 205-216.

Plášil, J., Kampf, A.R., Kasatkin, A.V. and Marty, J. (2014) Bluelizardite, $Na_7(UO_2)(SO_4)_4Cl(H_2O)_2$, a new uranyl sulfate mineral from the Blue Lizard mine, San Juan County, Utah, USA. *Journal of Geosciences*, **59**, 145-158.

Robie, R.A., Hemingway, B.S. and Fisher, J.R. (1978) Thermodynamic properties of minerals and related substances at 298.15 k and 1 bar (10/sup 5/pascals) pressure and at higher temperatures. Pp. 1-456. In: *U.S. Geological Survey Bulletin 1452*. U.S. Geological Survey, Washington DC, USA.

Sharifironizi, M. and Burns, P.C. (2018) Investigation of the structural stability of zippeite-group minerals using high-temperature calorimetry. *The Canadian Mineralogist*, **56**, 7-14.

Sharifironizi, M., Szymanowski, J.E.S., Sigmon, G.E., Navrotsky, A., Fein, J.B. and Burns, P.C. (2016) Thermodynamic studies of zippeite, a uranyl sulfate common in mine wastes. *Chemical Geology*, **447**, 54-58.

Sheldrick, G. (2008) Sadabs-2008/1–bruker axs area detector scaling and absorption correction. Bruker AXS. Madison, WI, USA.

Sheldrick, G.M. (2015a) Crystal structure refinement with SHELXL. *Acta Crystallographica*, **C71**, 3-8.

374 Sheldrick, G.M. (2015b) SHELXT–integrated space-group and crystal-structure determination.
375 *Acta Crystallographica*, **A71**, 3-8.
376 Shvareva, T.Y., Mazeina, L., Gorman-Lewis, D., Burns, P.C., Szymanowski, J.E., Fein, J.B. and
377 Navrotsky, A. (2011) Thermodynamic characterization of boltwoodite and uranophane:
378 Enthalpy of formation and aqueous solubility. *Geochimica et Cosmochimica Acta*, **75**,
379 5269-5282.
380 Simoncic, P. and Navrotsky, A. (2007) Systematics of phase transition and mixing energetics in
381 rare earth, yttrium, and scandium stabilized zirconia and hafnia. *Journal of the American*
382 *Ceramic Society*, **90**, 2143-2150.
383 Spano, T.L., Dzik, E.A., Sharifironizi, M., Dustin, M.K., Turner, M. and Burns, P.C. (2017)
384 Thermodynamic investigation of uranyl vanadate minerals: Implications for structural
385 stability. *American Mineralogist*, **102**, 1149-1153.
386 Tessier, F., Navrotsky, A., Le Sauze, A. and Marchand, R. (2000) Thermochemistry of
387 phosphorus oxynitrides: Pon and linapon glasses. *Chemistry of Materials*, **12**, 148-154.
388 Zhang, L., Lobeck, H.L., Dzik, E.A., Sigmon, G.E. and Burns, P.C. (2019) Thermochemical
389 study of tetravalent metal sulfate tetrahydrates: $A^{4+}(SO_4)_2(H_2O)_4$ (A^{4+}= Zr, Ce, U).
390 *Journal of Solid State Chemistry*, **276**, 56-60.

391 Chen, F., Ewing, R.C., and Clark, S.B. (1999) The Gibbs free energies and enthalpies of
392 formation of U^{6+} phases: An empirical method of prediction. *American Mineralogist*,
393 **84**(4), 650-664.
394